

Horizontal Magnetic Fields in the Solar Photosphere

V.A. Sheminova

Main Astronomical Observatory, National Academy of Sciences of Ukraine
27 Akademika Zabolotnogo st., Kyiv, 03680 Ukraine
E-mail: shem@mao.kiev.ua

Abstract

The results of 2D MHD simulations of solar magnetogranulation are used to analyze the horizontal magnetic fields and the response of the synthesized Stokes profiles of the FeI $\lambda 1564.85$ nm line to the magnetic fields. Selected 1.5-h series of the 2D MHD models reproduces a region of the network fields with their immediate surrounding on the solar surface with the unsigned magnetic flux density of 192 G. According to the magnetic field distribution obtained, the most probable absolute strength of the horizontal magnetic field at an optical depth of $\tau_5 = 1$ (τ_5 denotes τ at $\lambda = 500$ nm) is 50 G, while the mean value is 244 G. On average, the horizontal magnetic fields are stronger than the vertical fields to heights of about 400 km in the photosphere due to their higher density and the larger area they occupy. The maximum factor by which the horizontal fields are greater is 1.5. Strong horizontal magnetic flux tubes emerge at the surface as spots with field strengths of more than 500 G. These are smaller than granules in size, and have lifetimes of 3.6 min. They form in the photosphere due to the expulsion of magnetic fields by convective flows coming from deep subphotospheric layers. The data obtained qualitatively agree with observations with the Hinode space observatory.

1 Introduction

Recent spectropolarimetric observations using the Hinode satellite [17] have revealed unexpected properties of the magnetic fields in the quiet Sun. Horizontal fields proved to have larger magnetic flux densities and occupy larger areas on the solar surface than vertical fields [18, 19]. Information in the literature about the properties of horizontal magnetic fields in the solar photosphere is relatively sparse. Such fields were first observed in inter-network photospheric regions as short-duration (5 min) phenomena related to the decay of emerging weak bipolar magnetic fluxes [20]. The results of a Stokes-profile inversion [22] confirmed the presence of horizontal fields and demonstrated that weak horizontal fields should be present in quiet regions along with relatively strong vertical fields. Later, horizontal fields were detected in low-lying photospheric loops (bipoles) [6, 7, 24, 25] and in unipolar loops of emerging magnetic flux [26]. Magnetographic full disk observations of the Sun [15] also detected many horizontal fields in the quiet photosphere and their time variations. In addition, isolated small-scale islands of strong horizontal fields were recently observed in facular areas (plages) [16].

The currently available observational results lead to the following conclusions about the properties of horizontal magnetic fields in the solar photosphere.

(1) Horizontal fields are ubiquitous at the surface of the quiet Sun. They occupy a larger area than vertical fields, and are located nearer the edges of granules and inter-granular lanes.

(2) The structures in the horizontal fields are typically somewhat smaller than granules and larger than structures in the vertical fields.

(3) The horizontal fields are spatially separated from the vertical fields.

(4) The flux density of the horizontal component of the magnetic field in the inter-network regions (55 G) is a factor of five higher than the flux density of the vertical component (11 G).

(5) Strong horizontal fields in plages appear as small islands with strengths reaching 580 G.

What is the source of the abundant horizontal fields at the solar surface? How are the horizontal fields related to the vertical fields? What is the height variation of the horizontal fields in the photosphere? How are they distributed over the surface? How strongly are they coupled with penetrative convection processes? What is the nature of the horizontal photospheric fields? These questions can be addressed by magnetohydrodynamical (MHD) simulations of photospheric regions. No detailed analyses of the properties of the horizontal fields based on MHD simulations has been done [12, 13, 14, 31], and interest in these fields has been revived with the availability of Hinode observations. New three-dimensional (3D) simulations of inter-network fields in the quiet photosphere were carried out recently in [37]. According to the results obtained for a level of mean optical depth, $\tau = 1$, horizontal fields with strengths of >50 G cover an area a factor of three larger than the area covered by vertical fields with the same strengths. A local maximum of the horizontal field component is located near the temperature minimum (≈ 500 km). The strength of the horizontal field component exceeds that of the vertical component by factors of 2.0 or 5.6, depending on the initial conditions of the simulations. The horizontal fields are strongly coupled with penetrative convection.

Three-dimensional MHD simulations of local dynamo processes in subsurface solar layers were carried out in the subsequent study [32]. An analysis of the magnetic fields demonstrated that the horizontal field component dominates the vertical component in the height range where the photospheric spectral lines form. The ratio of the two components corresponded to the observed value. Magnetic fields of mixed polarities produced by a local dynamo mechanism near the surface are the main source of horizontal fields at the surface of the quiet Sun. Analyzing some other possible mechanisms [32], it was also noted that the formation of horizontal fields in the photospheric network and plages is affected more by the recirculation of the overall background granulation flux than by dynamo processes.

Our aim here is to analyze photospheric horizontal fields in the region of the photospheric magnetic network using two-dimensional (2D)MHD models made by Gadun [10, 12, 13], in order to answer some questions concerning their properties and nature.

In Section 2, we briefly describe the 2D MHD models, our analysis of the horizontal fields based on data of simulated magnetoconvection is presented in Section 3, the synthesized Stokes profiles are analyzed in Section 4, Section 5 presents comparisons with observations and a brief discussion, and Section 6 summarizes our conclusion.

2 MHD models of magnetogranulation

Realistic MHD models of photospheric regions are self-consistent models obtained by solving a system of radiative MHD equations. They can be used to synthesize spectral lines without any additional parameters such as the microturbulent and macroturbulent velocities. A review of the most recent results of MHD simulations can be found in [38]. Two-dimensional simulations of the solar convection have been actively developed in parallel with 3D simulations since 1984. Although 2D models cannot realistically reproduce convective flows [1], they reproduce many characteristics of 3D convection quite adequately [11, 27] and are useful in studying the properties of small-scale magnetic elements in the solar photosphere [2, 10, 13, 14, 35].

Among the known 2D MHD models for the solar magnetogranulation [2, 5, 8, 12, 14], Gadun's models [10, 12, 13] have proven to be fairly successful. They reproduced for the first time the small-scale magnetic fields of mixed polarities outside the active regions in the solar photosphere (see for details [10]). Based on these models, a close relationship between the strength and inclination angle of the photospheric magnetic fields and the predominance of horizontal fields were inferred [13]. This agrees with observations [24] obtained using the Advanced Stokes Polarimeter (ASP). Further, first evidence for the recirculation of convective flows near the surface was found [29], and later confirmed by 3D MHD simulations [39]. Using the 2D MHD models for Stokes diagnostics predicted specific changes in the Stokes profiles of the FeI λ 1564.8 nm line during the convective collapse of magnetic tubes [35], which was soon confirmed by observations with the Tenerife Infrared Polarimeter (TIP) [4]. Gadun's models made it possible to explain the observed anomalous asymmetry of the Stokes profiles of the FeI λ 630.2 nm line [28, 33] and investigate the distribution of the vertical magnetic-field component in regions with varying magnetic-flux densities at the solar surface, outside active regions [34].

The active development of new, improved 3D MHD models for the solar magnetoconvection is currently underway [31, 37, 40, 41]; however, they cannot yet answer all of the numerous questions that arise when interpreting the observational results [38]. Therefore, using the 2D MHD magnetogranulation models to study the small-scale structure of magnetic fields remains important.

The series of 2D MHD models are used in this paper was obtained by solving a full system of radiative MHD equations for a compressible, gravitationally stratified, turbulent medium [12]. Free boundary conditions admitting material inflow or outflow were specified for the velocities and thermodynamic quantities at the top and bottom boundaries. The corresponding boundary conditions for the magnetic field were $B_{hor} = 0$, $\partial B_{ver}/\partial z = 0$. The side boundary conditions were assumed to be periodic, which corresponds to multiple mirror reflections of the simulation domain in both horizontal directions. The simulation domain was located at heights ranging from 685 km above to 1135 km below the surface level, $Z = 0$ km. The horizontal size of the domain was about 4000 km, which corresponds to $5.5''$ on the solar disk. The spatial step was 35 km. The MHD simulations started by introducing a bipolar magnetic field in a previously computed two-dimensional hydrodynamic (2D HD) thermal-convection model. The initial unsigned magnetic flux was 54 G throughout the simulation domain. Within 30 min after the beginning of the simulations, the magnetic field comes into consistency with the convective motions of the plasma. Therefore, for further analyses, sampled MHD models can be used starting from a time of 30 min. More details of the numerical 2D MHD simulations can be found in [10, 12, 13].

The mean magnitudes of the vertical and horizontal components of the simulated mag-

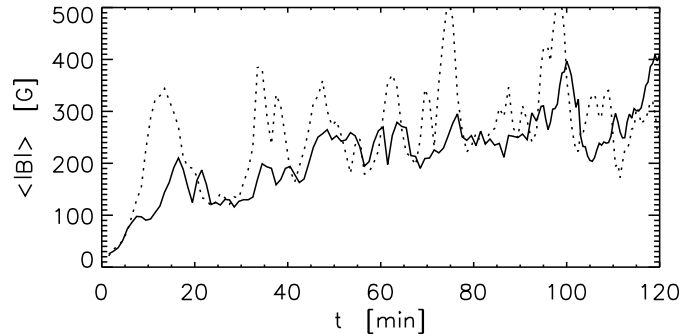


Figure 1: Simulated mean magnetic-field strength at the level $\tau_5 = 1$ as a function of time in the series of 2D MHD models. The solid curve shows $\langle |B_{ver}| \rangle$ and the dashed curve $\langle |B_{hor}| \rangle$.

netic field at an optical depth at λ 500 nm of $\tau_5 = 1$ grow rapidly with time, and fluctuate appreciably (Fig. 1). The flux density of the horizontal field at the surface increases due to the expulsion of field from deep layers by convective flows and its accumulation in the upper layers of granules. Further, the flux densities of the horizontal fields decrease sharply, since the fields flow into intergranular lanes and become nearly vertical. In narrow intergranular lanes, convective collapse comes into action after the vertical fields reach their equipartition level, and can either enhance the vertical fields in magnetic tubes to 2000 G or completely destroy these tubes. A detailed analysis of magnetoconvection [10] demonstrates that the flux density increases and oscillations in the magnetic flux are due to repeated penetrative-convection processes. One specific example of local recirculation of the granulation flux in the considered 2D MHD models is discussed in detail in [29].

Figure 2 shows the spatial and temporal variations in the magnetic field, velocity field, and radiation field at the $\tau_5 = 1$ level for the series of 2D MHD magnetogranulation models. The spatial-temporal image of the continuum intensity, I_c , represents the evolution of the granulation. Light regions (granules) can be seen between dark, twisted strips (intergranular lanes). The fragmentation of the granules, i.e., the separation of large granules into two smaller ones, is pronounced. We can clearly see that the horizontal size of the granules decreases as the magnetic flux increases in the simulation domain. The vertical velocity field, V_{ver} , closely resembles the corresponding diagram for the continuum intensity, since the radiation intensity and the line-of-sight velocity at the solar surface are strongly correlated. Note that the 5-minute oscillations of the line-of-sight velocity are more pronounced than the intensity oscillations. To trace the behavior of horizontal matter flows and their relationship to the granulation, we also show contours of the intergranular lanes in the plot of the horizontal velocities V_{hor} . The matter spreads from the centers to the edges of the granules. The horizontal flow velocities are substantially enhanced at the edges of magnetic tubes located in the intergranular lanes.

The plots of the vertical, B_{ver} , and horizontal, B_{hor} , components of the magnetic field shown to the right in Fig. 2 are shown using the same scale for the field strengths, to make these values and the areas occupied by them easily comparable. There are substantial differences between the vertical and horizontal fields, in both the shapes of structures and magnetic flux densities. Islands of strong horizontal fields are present in granules, mostly relatively close to intergranular lanes. As a rule, islands located at the centers of granules emerge before the fragmentation of the granule and the formation of new magnetic tubes. We described the processes of granular fragmentation in detail earlier in [12, 13]. The plot of the magnetic-field polarity, γ , demonstrates strong small-scale mixing of magnetic

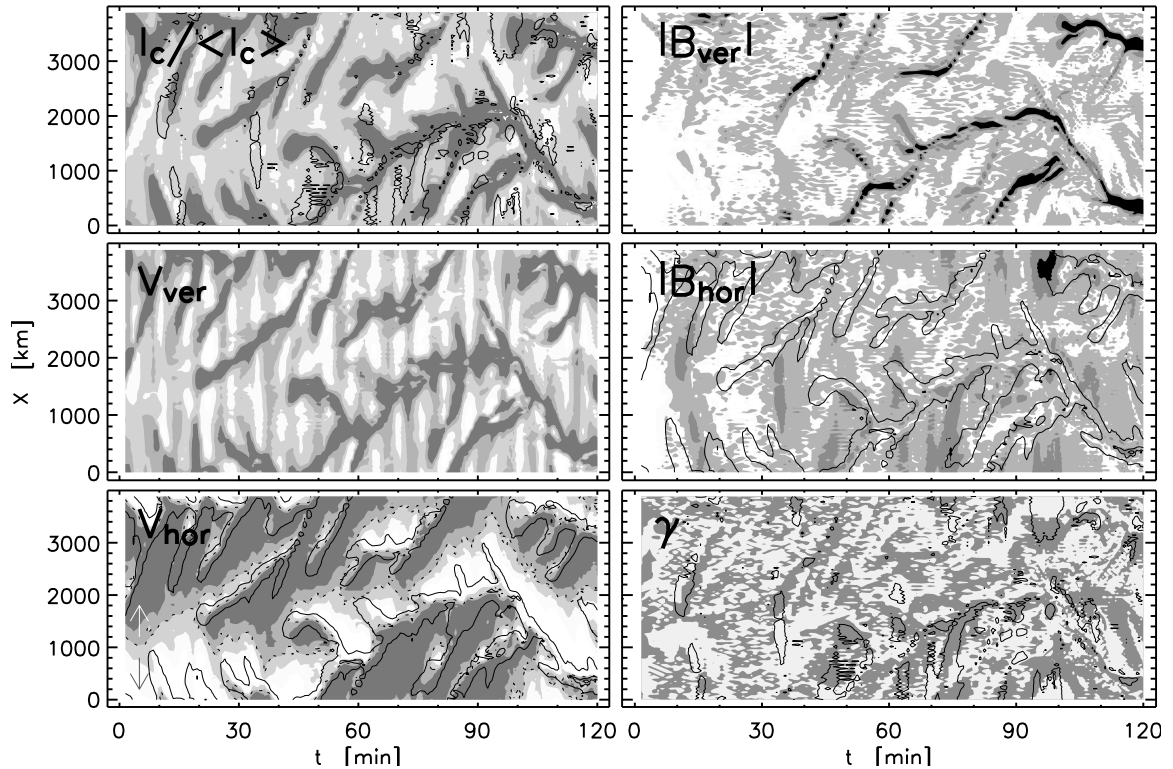


Figure 2: Spatial and temporal evolution of the simulated 2D magnetogranulation at the continuum-formation level, $\tau_5 = 1$. The top left panel shows the relative intensity of the continuum at a wavelength of 500 nm, with the gray scale from dark to light corresponding to $I_c / \langle I_c \rangle$ values of <0.8 , $0.8-1$, $1-1.3$, and >1.3 . The contours indicate islands of horizontal fields with $500 \text{ G} < |B_{hor}| < 1000 \text{ G}$. The middle left panel shows the line-of-sight velocity V_{ver} with the gray scale from dark (descending flows) to light (ascending flows) corresponding to V_{ver} values of <-1.5 , $-1.5-0$, $0-1.5$, and $>1.5 \text{ km/s}$. The bottom left panel shows the horizontal velocity V_{hor} ; the gray scale is similar to that for V_{ver} . The arrows near the lower left corner indicate the directions of the matter flow. The contours mark regions of intergranular lanes, and the dashed curve corresponds to $V_{hor} = 0$. The top right panel shows the magnitude of the vertical component, with the gray scale from light to dark corresponding to $|B_{ver}|$ values of <100 , $100-500$, $500-1000$, and $>1000 \text{ G}$. The middle right panel shows the magnitude of the horizontal component; the gray scale is similar to that for $|B_{ver}|$. The contours mark regions of intergranular lanes. The bottom right panel shows the inclination angle, γ , of the magnetic field; light gray shows positive and dark gray negative values. The contours indicate islands of horizontal fields.

fields directed toward and from the observer.

Strong vertical magnetic concentrations are clearly visible after the first 30 min of the simulations in the top right panel of Fig. 2. Their outlines resemble the observed magnetic structures of the photospheric supergranular network, which are surrounded by weaker, mixed fields. In addition, the flux density of the vertical magnetic field at the $\tau_5 = 1$ level in the region of the simulated magnetogranulation is close to the value observed in the vicinity of the photospheric network [23]; i.e., it is an order of magnitude higher than the flux density in inter-network areas. The amplitudes of the Stokes profiles of spectral lines computed for the given simulation domain are also an order of magnitude larger than the amplitudes measured in inter-network regions. We thus conclude that our simulations have reproduced the emergence of magnetic flux through the photosphere in

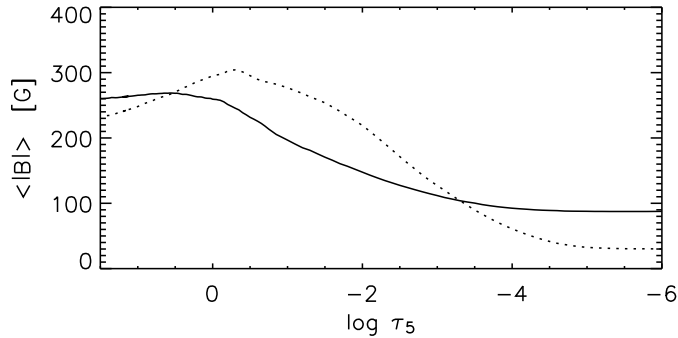


Figure 3: Mean magnitudes of the horizontal and vertical components of the magnetic field in the 1.5-h series of 2D MHD models as a function of the height in the photosphere. The solid curve shows $\langle |B_{ver}| \rangle$, and the dashed curve $\langle |B_{hor}| \rangle$.

network rather than inter-network areas.

Our analysis is based on a 1.5-h series of 2D MHD models (starting from the first 30 min of the simulations). The time resolution is 1 min during the first hour and 0.5 min during the subsequent 30 min. This series forms 126 2D models, which, in turn, contain 112 1D models each. In total, we have 14 112 magnetic-field measurements, enabling a statistical analysis of the simulation data with the aim of revealing the properties of the horizontal fields. We emphasize that, according to [30], the spatial resolution of the numerical MHD simulations corresponds to two or three steps of the computational grid. For our series of 2D MHD models, the resolution is 100 km, or $0.15''$.

3 Properties of the horizontal magnetic fields

Figure 3 shows the strengths of the vertical, $|B_{ver}|$, and horizontal, $|B_{hor}|$, components averaged over space and time for the 1.5-h series of 2DMHD models as a function of optical depth. The mean strength of the horizontal field in the photosphere is higher than the mean strength of the vertical field down to the level $\log \tau_5 \approx -3.5$ ($Z \approx 400$ km). The maximum excess, $\langle |B_{hor}| \rangle / \langle |B_{ver}| \rangle \approx 1.5$, is substantially less than is observed for the inter-network areas of the quiet Sun [19].

The probability-density function (PDF) is frequently used to investigate the distribution of the magnetic-field strength over the surface [9]. Figure 4 shows the PDFs obtained for $|B_{ver}|$, $|B_{hor}|$, and the inclination of the magnetic-field vector, γ , at the $\tau_5 = 1$ level. The most probable values for $|B_{ver}|$, $|B_{hor}|$, and γ are 50 G, 50 G, and 87° , and the corresponding mean values are 192 G, 244 G, and 64° , respectively. Hence, the factor by which the horizontal exceeds the vertical field component averaged over the domain at the $\tau_5 = 1$ level is 1.3.

Following [9], we calculate the filling factor α based on the obtained PDFs, which determines the fractions of the surface occupied by weak, moderate, and strong fields, which we arbitrarily define as fields with strengths $|B_{hor}| < 500$ G, $500 \leq |B_{hor}| < 1000$ G, and $|B_{hor}| \geq 1000$ G. We apply similar definitions to the vertical fields. Note that, in contrast to the observed patterns, the surface of the simulation domain is completely covered with magnetic field, i.e., the magnetic-field filling factor is unity. In addition to α , we also calculated the fractions of weak, moderate, and strong fields in terms of their magnetic fluxes ϕ and the fractions of the magnetic energy associated with them relative to the total magnetic energy ε . The results of our calculations in the total magnetic

Table 1: Percentages of weak, moderate, and strong magnetic fields in the 1.5-h series of 2D MHD models in terms of their occupied areas on the surface of the simulation domain (α), their densities (ϕ), and the magnetic energy they produce (ε).

Strength, G	α (%)	ϕ (%)	ε (%)
$ B_{hor} < 500$	72	28	15
$500 \leq B_{hor} < 1000$	18	20	30
$ B_{hor} \geq 1000$	10	2	5
$ B_{ver} < 500$	67	25	8
$500 \leq B_{ver} < 1000$	9	12	12
$ B_{ver} \geq 1000$	24	13	30

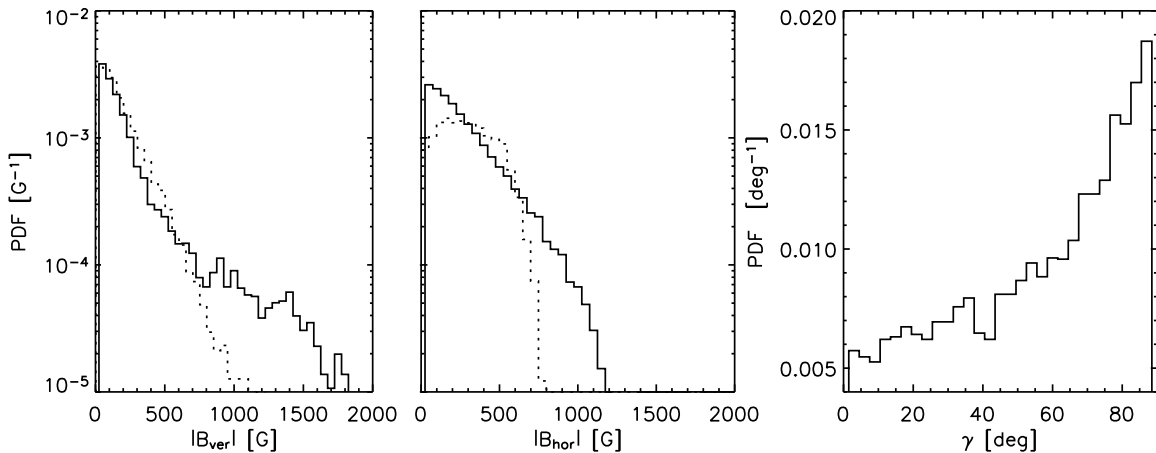


Figure 4: Histograms of the probability-density functions (PDFs) for the strengths of the vertical and horizontal components of the magnetic field and the inclinations of the magnetic vector in the 1.5-h series of MHD models at the $\tau_5 = 1$ level. The solid curve shows the MHD-simulation data, and the dotted curve the Stokes-diagnostic data.

energy are given in the table. These indicate that weak horizontal fields in the simulated region of the photospheric network occupy a larger area (72%) and have a higher flux density (28%) than the other fields. Relatively large contributions are given by moderate horizontal and strong vertical fields (30% each). The moderate horizontal fields can be seen as small islands in Fig. 2 (second plot on the right). These are mainly bipolar, and their lifetimes are 3-6 min. In many cases, such islands emerge in regions next to intergranular lanes rather than in the central parts of the granules.

Strong horizontal fields cover 10% of the total surface area, while strong vertical fields cover 24%. An island of strong horizontal field is clearly visible in Fig. 2 (second plot on the right) in a large granule, shortly before its fragmentation. In contrast to strong horizontal fields (or horizontal tubes), strong vertical fields (or vertical tubes) are concentrated in intergranular lanes (Fig. 2, first plot on the right). These fields form a network of strong vertical fields in the simulation domain, similar to the observed fields of the photospheric network represented by magnetograms.

Let us consider the properties of the horizontal fields in the simulation domain using the statistical dependences of B_{hor} on the granulation parameters (Fig. 5). The relationship of the horizontal fields to the granulation reflects the dependence of B_{hor} on the contrast of the continuum emission, $I_c / \langle I_c \rangle$. In the figure, I_c is the continuum inten-

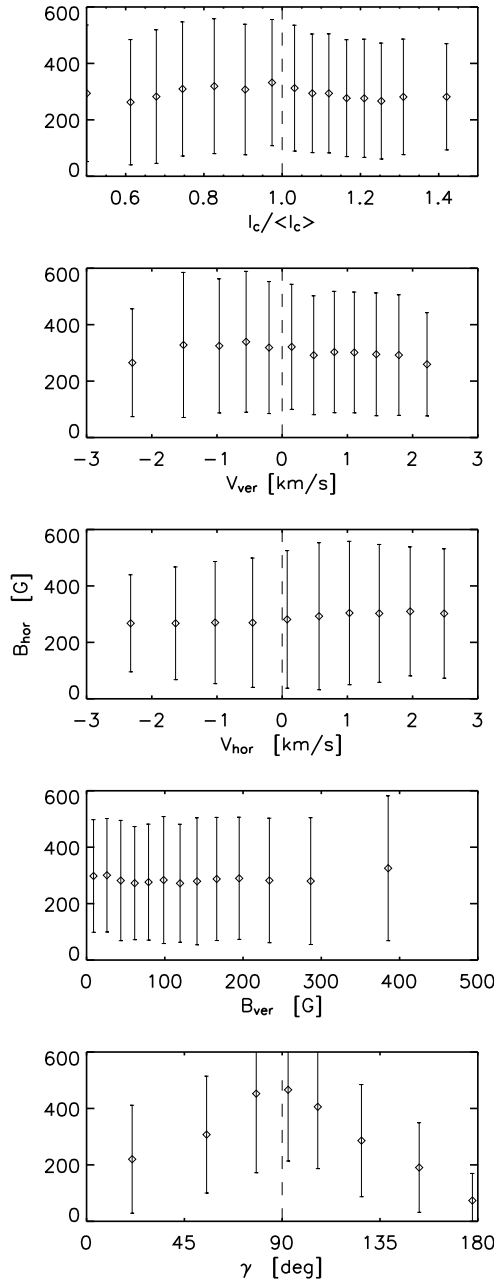


Figure 5: Statistical dependences of the strengths of the horizontal magnetic-field component on the parameters characterizing the granulation and magnetic field. Positive V_{ver} correspond to upflows and negative V_{ver} to downflows. The values are averaged over the same number of points (881) in each interval. The vertical bars indicate the standard deviation (the spread of values) in each averaging interval. The rms error of each averaged value of B_{hor} is typically <10 G.

sity at λ 500 nm at each computation point, and $\langle I_c \rangle$ is the intensity I_c averaged over the simulation domain for a particular time. No pronounced dependence can be seen, although stronger horizontal fields exhibit some tendency to correspond to contrasts of $I_c / \langle I_c \rangle \approx 1$ or somewhat less. The dependence of B_{hor} on the line-of-sight velocity V_{ver} is also not clearly expressed, and there is only a weak tendency for B_{hor} to increase in granulation areas with slow, descending matter flows. There is virtually no relationship between B_{hor} and the horizontal component of the velocity field. Similarly, B_{hor} and B_{ver} are uncorrelated. The dependence of B_{hor} on the inclination γ indicates a strong relationship between them, with the strength of the horizontal component being, on average, about 500 G for the most inclined, nearly horizontal fields and about 200 G for weakly inclined fields (on average, $\gamma = 20^\circ$). Thus, the statistical dependences do not reveal any close relationships between the horizontal fields and the granulation and vertical fields. The moderate and strong horizontal and vertical fields are spatially separated.

4 Stokes diagnostics of the magnetic fields

To analyze the response of the linear and circular Zeeman polarization to the magnetic fields, we considered synthesized Stokes profiles (I , Q , U , V) of the FeI λ 1564.8 nm line. These profiles were obtained along the line of sight for the 1.5-h series of MHD models at any point of the simulated surface, in accordance with observations at the center of the solar disk. The spectral resolution was 5 mÅ within ± 1.5 Å of the line center. The iron abundance was chosen to be $A_{Fe} = 7.43$, the oscillator strengths $\log gf = -0.675$, and the excitation potential of the lower level $EP = 5.43$ eV. The Van der Waals damping constant was computed using the formulas given in [3]. The computations were carried out using the SPANSATM code [36]. Analogous to the interpretation of observations described in [19], we obtained V_{tot} and Q_{tot} from the synthesized Stokes V and Q profiles by integrating V and Q over the wavelength:

$$V_{tot} = \text{sgn}(V_b) \frac{|\int_{\lambda_b}^{\lambda_0} V(\lambda) d\lambda| + |\int_{\lambda_0}^{\lambda_r} V(\lambda) d\lambda|}{I_c \int_{\lambda_b}^{\lambda_r} d\lambda},$$

$$Q_{tot} = \frac{\int_{\lambda_b}^{\lambda_r} |Q(\lambda)| d\lambda}{I_c \int_{\lambda_b}^{\lambda_r} d\lambda}.$$

Here, $\text{sgn}(V_b)$ is the sign of the blue peak amplitude of the V profile, λ_0 the central wavelength of the line, and λ_b and λ_r the limits for integration over the full line profile. Note that the intensity of the Stokes U profile is nearly zero in 2D MHD simulations, and we did not include it when calculating the total linear polarization.

To convert the computed V_{tot} and Q_{tot} values into field strengths, we determined the dependences of V_{tot} and Q_{tot} on B_{ver} and B_{hor} . The strengths B_{ver} and B_{hor} were deduced from 2D MHD models at the $\log \tau_5 = -1$ level. According to our calculations, this is the photospheric level that corresponds, on average, to the effective formation depth of the Stokes profiles of the FeI λ 1564.8 nm line. The calibration curves are shown in Fig. 6. We used these to obtain the magnetic flux density for the horizontal, B_{hor} , and vertical, B_{ver} , components from each pair of synthesized V and Q profiles and to construct the corresponding PDFs (Fig. 4, dotted curve). These differ substantially from the PDFs obtained from direct measurements of B_{ver} and B_{hor} using the MHD models (solid curve). According to the PDFs based on the Stokes profiles, the most probable strengths of the

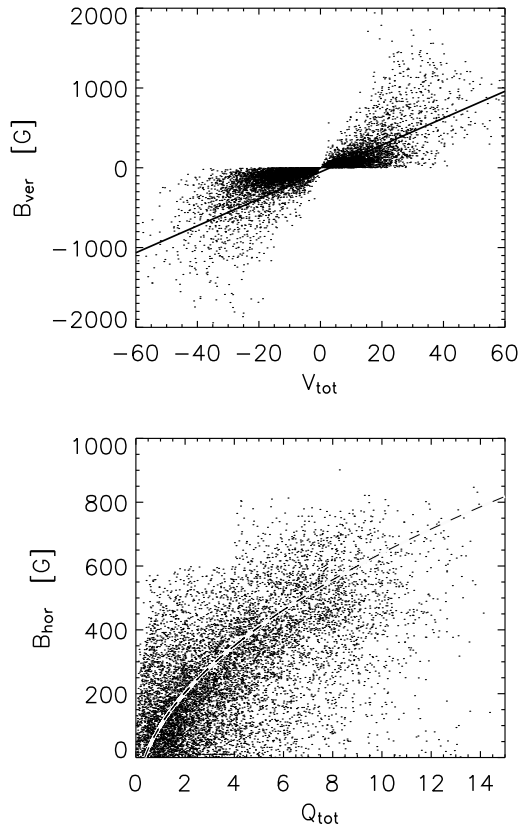


Figure 6: Calibration curves based on the 2D MHD simulations of B_{ver} and B_{hor} and the synthesized Stokes profiles of the FeI $\lambda 1564.8$ nm line for which the circular (V_{tot}) and linear (Q_{tot}) polarizations were calculated in mÅ.

horizontal and vertical magnetic-field components are 174 and 28 G, while the mean values are 310 and 188 G, respectively. The factor by which the mean horizontal exceeds the mean vertical field strength is 1.6. Recall that direct measurements using MHD models yielded 50 and 50 G, 244 and 192 G, and 1.3. The horizontal-excess factor deduced from the Stokes profiles is slightly higher than the factor obtained from the MHD data because the calibration curves overestimated the flux density of the horizontal fields. This means that the calibration of the linear-polarization signals introduces an additional error in estimates of the strength of the horizontal field.

According to the analysis of two series of 3D MHD models of inter-network regions presented in [37], the horizontal-excess factors were 2.0 and 5.6 (MHD data) and 1.5 and 2.8 (Stokes diagnostics), i.e., the Stokes-based factors were smaller than the simulated factors. In the analysis of [37], the linear-polarization signals in the inter-network regions are an order of magnitude weaker than in magnetic-network fields. This could also affect the accuracy of the Stokes diagnostics and calibration.

5 Comparisons with observations

According to spectropolarimetry observations carried out on the Hinode satellite with a spatial resolution of $0.3''$, the flux density of the horizontal magnetic-field component in inter-network regions is about 55 G [18, 19], and reaches 580 G [16] in the plages. The mean magnitude of the horizontal-field strength for our simulated domain, which probably represents a region of the observed supergranular photospheric network and its immediate

vicinity, is 244 G. We believe that this is consistent with the observations.

Let us compare the available observational data for both inter-network regions and the plages with the results of our analysis. According to our 2D MHD simulations, the magnitude flux density of the horizontal magnetic field exceeds that of the vertical field by, on average, a factor of 1.3 (with the maximum factor being 1.5). This is much less than the value derived from observations of inter-network regions (a factor of 5 [19]). The smaller factor we have obtained in the simulated photospheric-network region may be due to the higher density of strong, small-scale, vertical network magnetic fields (magnetic flux tubes) in the simulation domain, compared to the observed inter-network quiet regions.

Observations of the plages [16] revealed the emergence of isolated horizontal fields in the form of small islands $1.4'' \times 1''$ in size with lifetimes of about 6 min. These appear inside a granule and gradually move to the intergranular lanes, later leaving the field of view. The inversion of the Stokes profiles observed in these islands indicates that the horizontal field can reach 580 G. According to our results, islands of strong horizontal fields with similar sizes and lifetimes and with strengths of $500 \text{ G} > B_{hor} > 1000 \text{ G}$ also emerge inside granules at the surface of the simulation domain (Fig. 2, second plot on the right). In addition, we detected an island of strong field with $B_{hor} > 1000 \text{ G}$, $X = 3600 \text{ km}$, and $t = 95.5 \text{ min}$.

Figure 7 shows a snapshot of the vertical cross section of the simulation domain at the site where an island of strong horizontal fields is forming. At time $t = 95.5 \text{ min}$, two strong horizontal tubes and two strong vertical tubes can be seen. The convective motions penetrating from lower subphotospheric layers carry magnetic fields to middle and upper photospheric layers; this is the effect of so-called magnetic flux expulsion, described in detail in [32, 37]. A further growth of the field strength in the horizontal tube that has formed on the surface of a granule occurs under the action of the cool, denser matter located over the large granule. The magnetic field lines condense and start to bend. The cloud of cool material gradually sinks, entraining magnetic-field lines. The large granule begins fragmenting, and this pumps the strong horizontal field into deeper layers, forming a new vertical tube [10, 13].

It follows from our 2D MHD simulations that strong horizontal tubes do not rise to upper photospheric layers (Fig. 7). Therefore, the mean flux density excess of the horizontal over the vertical component, shown in Fig. 1, is basically manifest in the lower and middle photosphere. For the same reason, the area occupied by strong horizontal tubes at the $\tau_5 = 1$ level far exceeds the area of strong vertical tubes.

The response of the synthesized Stokes profiles of the iron $\lambda 1564.8 \text{ nm}$ line to horizontal and vertical fields in the 1.5-h series of MHD models yields a horizontal-excess factor of 1.6. This is a factor of three smaller than the value obtained from observed Stokes profiles of the $\lambda 630.2 \text{ nm}$ iron line [19] in internetwork regions. The main reason for the disagreement between the observations and our simulations appears to be the difference in the magnetic fluxes for the observed and simulated regions. On the other hand, our horizontal-excess factor is not very different from the factors of 1.5 and 2.8 found in [37] using the synthesized Stokes profiles of the FeI $\lambda 630.2 \text{ nm}$ line and two series of 3D MHD models of internetwork regions. The simulation results for internetwork fields of [37] do not satisfactorily reproduce the factor of 5 obtained in [19], although the magnetic flux density in the 3D MHD models is similar to the values derived from observations. One possible reason for this disagreement is insufficient accuracy in the calibration of the observed linear-polarization signals. We also cannot rule out the possibility that the vertical magnetic flux density was underestimated in the observations of [19], which had a spatial resolution of $0.3''$ (or about 200 km). This could result if the contributions of

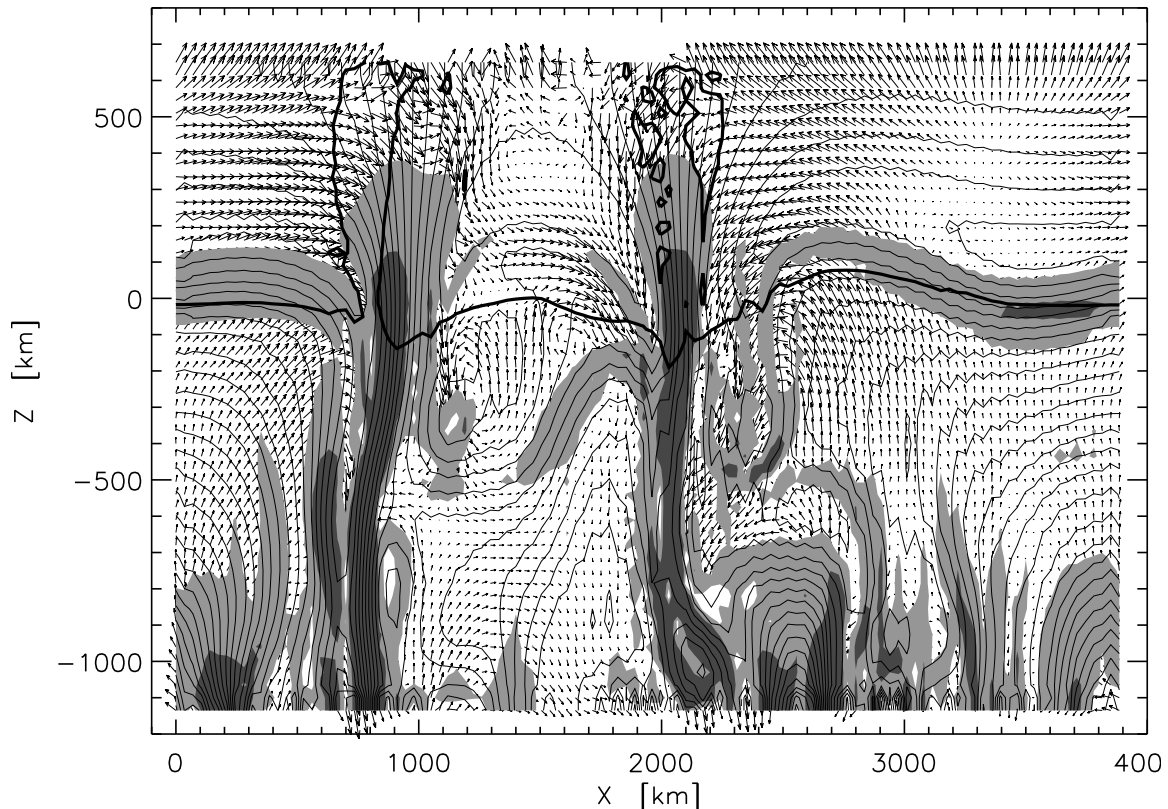


Figure 7: Snapshot of the vertical cross section of the simulation domain for $t = 95.5$ min. The heavy curve shows the isotherm for $T = 5500$ K, which approximately indicates the level of the mean optical depth of $\tau \approx 1$, while the light solid curves show magnetic-field lines. The gray shading shows vertical and horizontal fields with strengths from 500 to 1000 G, while dark gray corresponds to strengths above 1000 G. The arrows indicate the direction of the velocity of the matter flow at each computational grid point, and their length is proportional to the corresponding flow speed.

smaller magnetic structures with opposite field polarities partially cancel out, which was not taken into account in the estimates of the flux density.

Note also that the 2D MHD simulations of magnetoconvection that we use here have some limitations and drawbacks. The 2D representation of the granular motions is a very crude assumption. The matter-flow divergence in the 2D simulation domain occurs in a plane, which can affect the velocities and possibly the magnetic-field strengths. The magnetic tubes in our models form between two granules, while small-scale elements in the solar photosphere are observed in gaps joining three or more granules. The simulations deal only with the granular scale of the solar convection, and the initial magnetic field is artificially introduced in the models. To comprehend and trace the formation of magnetic-network regions, it would be desirable to take into account larger scales of the solar convection, such as the meso- and supergranulation scales. These drawbacks of the simulations could affect the quantitative estimates obtained. Thus, our conclusions below are based on the qualitative features of our results.

6 Conclusion

We have analyzed horizontal magnetic fields using a 1.5-h series of 2D MHD models of the solar magnetogranulation. The flux density of the vertical component of the magnetic field (about 200 G) in the spatial-temporal simulation domain corresponds to the mean magnetic flux density observed in regions of the photospheric supergranular network. This suggests that our series of models reproduces the region of the supergranular network and its immediate vicinity in the solar photosphere. Our simulation and Stokes-diagnostic results qualitatively agree with observations carried out on the Hinode satellite.

The main conclusions of our analyses are as follows.

(1) On average, the unsigned flux density of the horizontal magnetic-field component exceeds that of the vertical component at photospheric heights from 0 to 400 km.

(2) Weak magnetic fields with horizontal components < 500 G occupy a larger surface area at the $\tau_5 = 1$ level and make a larger contribution to the total magnetic energy than do fields whose vertical component is weaker than 500 G.

(3) Magnetic fields with horizontal components ranging from 500 to 1000 G are concentrated in small islands in the regions between granules and intergranular lanes. These islands are bipolar in many cases. They are slightly smaller than the horizontal granular size, and have lifetimes of 3–6 min.

(4) The fragmentation of a large granule is preceded by the formation of a strong horizontal tube with field strength $B_{hor} > 1000$ G at the surface of the granule.

(5) The formation of horizontal magnetic fields is closely related to processes associated with penetrative convection, such as the expulsion of magnetic flux and the local recirculation of the granular flux. Their strength depends on the magnetic flux in the given region.

Acknowledgments The author thanks N.V. Kharchenko for discussions of the results, useful comments and advices.

References

- [1] M. Asplund, H.-G. Ludwig, Å. Nordlund, and R. F. Stein, *Astron. Astrophys.* 359, 669 (2000).
- [2] I. N. Atroshchenko and V. A. Sheminova, *Kinemat. Fiz. Nebesn. Tel* 12 (4), 32 (1996).
- [3] P. S. Barklem, N. Piskunov, and B. J. O'Mara, *Astron. Astrophys. Suppl. Ser.* 142, 467 (2000).
- [4] L. R. Bellot Rubio, R. Luis, I. Rodríguez Hidalgo, et al., *Astron. Astrophys.* 560, 1010 (2001).
- [5] P. N. Brandt and A. S. Gadun, *Kinemat. Fiz. Nebesn. Tel* 11 (4), 44 (1995).
- [6] R. Centeno, H. Socas-Navarro, B. Lites, et al., *Astrophys. J.* 666, L137 (2007).
- [7] B. De Pontieu, *Astrophys. J.* 569, 474 (2002).
- [8] W. Deinzer, G. Hensler, M. Schüssler, and E. Weisshaar, *Astron. Astrophys.* 139, 435 (1984).

- [9] I. Domínguez Cerdeña, J. Almeida Sánchez, and F. Kneer, *Astrophys. J.* 407, 741 (2003).
- [10] A. S. Gadun, *Kinemat. Fiz. Nebesn. Tel* 16 (2), 99 (2000).
- [11] A. S. Gadun, S. K. Solanki, and A. Johannesson, *Astron. Astrophys.* 350, 1018 (1999).
- [12] A. S. Gadun, V. A. Sheminova, and S. K. Solanki, *Kinemat. Fiz. Nebesn. Tel* 15 (5), 387 (1999).
- [13] A. S. Gadun, S. K. Solanki, V. A. Sheminova, and S. R. O. Ploner, *Solar Phys.* 203, 1 (2001).
- [14] U. Grossmann-Doerth, M. Schüssler, and O. Steiner, *Astron. Astrophys.* 337, 928 (1998).
- [15] J. W. Harvey, D. Branston, C. J. Henney, and C. U. Keller, *Astrophys. J.* 659, L177 (2007).
- [16] R. Ishikawa, S. Tsuneta, K. Ichimoto, et al., *Astron. Astrophys.* 481, L25 (2008).
- [17] T. Kosugi, K. Matsuzaki, T. Sakao, et al., *Solar Phys.* 243, 3 (2007).
- [18] B. Lites, H. Socas-Navarro, M. Kubo, et al., *Publ. Astron. Soc. Japan* 59, 571 (2007).
- [19] B. Lites, M. Kubo, H. Socas-Navarro, et al., *Astrophys. J.* 460, 1237 (2008).
- [20] B. Lites, K. D. Leka, A. Skumanich, et al., *Astrophys. J.* 460, 1019 (1996).
- [21] B. Lites, A. Skumanich, and V. Martinez Pillet, *Astron. Astrophys.* 333, 1053 (1998).
- [22] N. Meunier, S. K. Solanki, and W. C. Livingston, *Astron. Astrophys.* 331, 771 (1998).
- [23] B. W. Lites, *Astrophys. J.* 573, 431 (2002).
- [24] B. Lites, A. Skumanich, and V. Martinez Pillet, *Astron. Astrophys.* 333, 1053 (1998).
- [25] M. J. Martínez González, M. Collados, B. Ruiz Cobo, and S. K. Solanki, *Astron. Astrophys.* 469, L39 (2007).
- [26] D. Orozco Suárez, L. R. Bellot Rubio, J. C. del Toro Iniesta, et al., *Astrophys. J.* 670, L61 (2007).
- [27] S. R. O. Ploner, S. K. Solanki, and A. S. Gadun, *Astron. Astrophys.* 352, 679 (1999).
- [28] S. R. O. Ploner, M. Schüssler, S. K. Solanki, et al., in *Advanced Solar Polarimetry – Theory, Observation, and Instrumentation*, Ed. by M. Sigwarth, *ASP Conf. Ser.* 236, 371 (2001).
- [29] S. R. O. Ploner, M. Schüssler, S. K. Solanki, and A. S. Gadun, in *Advanced Solar Polarimetry. Theory, Observation, and Instrumentation*, Ed. by M. Sigwarth, *ASP Conf. Ser.* 236, 363 (2001).
- [30] J. Sánchez Almeida, *Astron. Astrophys.* 450, 1198 (2006).

- [31] W. Schaffenberger, S. Wedemeyer-Böhm, O. Steiner, and B. Freytag, in *Solar MHD Theory and Observations*, Ed. by J. Leibacher, R. E. Stein, and H. Uitenbroek, ASP Conf. Ser. 354, 345 (2006).
- [32] M. Schüssler and A. Vögler, *Astron. Astrophys.* 481, L5 (2008).
- [33] V. A. Sheminova, *Kinemat. Fiz. Nebesn. Tel* 21 (3), 172 (2005) [*Kinem. Phys. Celest. Bodies* 21, 120 (2005)].
- [34] V. A. Sheminova, *Solar Phys.* 254, 29 (2009).
- [35] V. A. Sheminova and A. S. Gadun, *Astron. Zh.* 77, 790 (2000) [*Astron. Rep.* 44, 701 (2000)].
- [36] V. A. Sheminova, *Calculating the Profiles of Stokes Parameters of Magnetoactive Absorption Lines in Stellar Atmospheres*, Dep. VINITI May 30, 1990, No. 2940-V90 (Kiev, Ukraina, 1990) [in Russian].
- [37] O. Steiner, R. Rezaei, W. Schaffenberger, and S. Wedemeyer-Böhm, *Astrophys. J.* 680, L85 (2008).
- [38] O. Steiner, in *Modern Solar Facilities. Advanced Solar Science*, Ed. by F. Kneer, K. G. Puschmann, and A. D. Wittmann (Universitätsverlag, Göttingen, 2007).
- [39] R. F. Stein and Å. Nordlund, in *IAU Colloquium 188: Magnetic Coupling of the Solar Atmosphere*, Ed. by H. Sawaya-Lacoste (ESA Publ. Division, 2002), p. 83.
- [40] A. Vögler, S. Shelyag, M. Schüssler, et al., *Astron. Astrophys.* 429, 335 (2005).
- [41] R. F. Stein and Å. Nordlund, *Astrophys. J.* 642, 1246 (2006).